Journal of Computational Physics **175,** 412–437 (2002)
doi:10.1006/jcph.2001.6899, available online at http://www.idealibrary.com on IDEAL®

Bounded Skew High-Order Resolution Schemes for the Discrete Ordinates Method

P. J. Coelho

Instituto Superior Técnico, Technical University of Lisbon, Mechanical Engineering Department, Av. Rovisco Pais, 1049-001 Lisbon, Portugal
E-mail: coelho@navier.ist.utl.pt

Received October 20, 2000; revised July 2, 2001

The discrete ordinates method for the solution of the radiative heat transfer equation suffers from two main shortcomings, namely ray effects and numerical smearing. Spatial discretization, which is the cause of numerical smearing, constitutes the subject of the present work. Bounded skew high-order resolution schemes are applied to the discrete ordinate equations and compared with standard bounded high-order resolution schemes (CLAM, MUSCL, and SMART), as well as with the step scheme. Calculations are performed for two- and three-dimensional enclosures with transparent, emitting–absorbing, and emitting–absorbing–scattering media. One of the walls of the enclosure is hot, while the others are cold. The results demonstrate that the bounded skew high-order schemes are more accurate than the bounded high-order ones, regardless of the radiative properties of the medium. The improved accuracy is more significant for the radiation intensity along directions oblique to the coordinate lines, but it is also observed for the incident radiation. The difference between the results of the skewed and the standard schemes is attenuated as the optical thickness of the medium increases. A drawback of the skewed schemes is their higher computational requirements, associated with an increased number of iterations required for convergence.

1. INTRODUCTION

Radiative heat transfer plays an important role in many relevant engineering problems, including, for example, combustion applications (fires, fossil fuel fired utility boilers, rocket nozzles and engines, etc.), solar energy systems, laser materials processing, and satellite and other space systems. Several numerical solution methods have been developed for radiative heat transfer problems, including the zone, the Monte Carlo, the spherical harmonics, the discrete transfer, the discrete ordinates, and the finite-volume methods [1]. Although the zone and the Monte Carlo methods are often considered the most accurate ones, their computational requirements are also the highest, and therefore none of the methods currently

0021-9991/02 $35.00

available can be considered the best one for all problems. The discrete ordinates method [2, 3], which is employed in the present work, has emerged in the last decade as one of the most popular methods, providing a good compromise between accuracy and computational economy.

The discrete ordinates method is based on the numerical solution of the radiative transfer equation along a set of discrete directions spanning the total solid angle range of 4π, replacing the integrals over direction by numerical quadratures. Two major shortcomings of this method that may strongly affect the solution accuracy are the ray effect and numerical smearing, which have been discussed in Refs. [4, 5]. The ray effect is associated with the angular discretization and arises from the approximation of the continuous angular variation of the radiation intensity field by a discrete set of radiation intensities in specified ordinate directions. It is independent of the spatial discretization. Ray effects may be mitigated by refining the angular discretization or by using the modified discrete ordinates method [6]. The numerical smearing, also referred to in the literature as numerical scattering or false scattering, is the counterpart of false diffusion in computational fluid dynamics (CFD). In fact, the radiative transfer equation can be interpreted as the convection of a scalar (the radiation intensity) in a prescribed velocity field (characterized by the direction cosines of the direction of propagation of radiation). There is a source term in the case of a participating medium, but no diffusion term. The numerical smearing is associated with the spatial discretization scheme, and it is independent of the angular discretization. It arises in multidimensional problems when the radiation beams are not aligned with the grid lines.

An evaluation of spatial discretization schemes employed in the discrete ordinates method has been presented in [7]. The two most widely used ones are the step and the diamond schemes, which are the counterparts respectively, of the upwind and the central differencing schemes in CFD. The great advantage of the step scheme is that physically unrealistic negative radiation intensities are never predicted. However, excessive numerical smearing is introduced by this scheme. The diamond scheme reduces the numerical smearing, but it may yield overshoots and undershoots of the boundary intensities, and negative intensities may appear. These negative intensities may be eliminated using the negative intensity fix-up procedure proposed in [2], which sets them to zero. However, spatially oscillating, physically unrealistic intensities may still occur. This problem is shared by the positive scheme [8], which ensures positive radiation intensities, but not necessarily bounded ones. Negative radiation intensities may also be prevented by using a variable weight scheme [9] that combines the step and the diamond schemes. The diamond scheme is used if negative intensities are not found. Otherwise, a weighted average of the two schemes is used, and the weight is selected by trial and error to enforce positive values. The exponential scheme is potentially more accurate in one-dimensional computations, but not in multidimensional ones, where unbounded solutions may occur, as discussed in [7].

All the spatial discretization schemes mentioned above treat the radiation across a control volume face as locally one dimensional. This means that the radiation intensity at a cell face is calculated from the radiation intensity at points that lie along the normal to the cell face. Other schemes have been proposed to account for the multidimensional nature of radiation (i.e., schemes that calculate the radiation intensity at a cell face based on the radiation intensity at points that lie along the direction of propagation of radiation). The simplest of these schemes is the modified exponential scheme [10], which integrates the radiative transfer equation along every direction assuming a constant source term. The upstream

location must be chosen carefully to avoid negative nodal intensities and wiggles. A similar scheme, which differs only in the evaluation of the upstream intensity, is presented in Ref. [11]. An improved high-order exponential scheme has been proposed in the formulation of the finite-volume method for radiative heat transfer [12]. The finite-volume method for radiative transfer has many similarities to the discrete ordinates method, and so this scheme is applicable to both methods. The interpolation of the upstream intensity from grid node values must be done carefully to ensure conservation. Similar high-order exponential schemes have been employed in [13, 14]. These authors use the discrete ordinates interpolation method, a modification of the standard discrete ordinates method which does not use the control-volume formulation. This allows greater flexibility in the calculation of the upstream radiation intensity, but does not ensure conservation of radiative energy. All these skewed schemes are potentially more accurate than the locally one-dimensional ones mentioned before. A skewed upwinding procedure has recently been proposed [15] in the framework of the control-volume finite-element method using triangular control volumes for two-dimensional problems. The scheme is stable and economical and it inherently precludes the possibility of computing negative coefficients in the discretized algebraic equations (i.e., negative intensities do not appear). It is more accurate than the step scheme but is still first-order accurate.

Bounded high-order resolution (HR) differencing schemes initially developed in the CFD community have also been applied to solve the radiative transfer equation using the discrete ordinates method. The SMART scheme [16] has been employed in [17], and the MINMOD [18], MUSCL [19], CLAM [20], and SMART schemes have been used in [21]. As in CFD, it has been shown that the radiation intensity field computed using these schemes is much more accurate than that obtained using the step scheme, the diamond scheme, and its modifications.

The HR schemes treat the radiation across a control-volume face as locally one-dimensional. Jessee and Fiveland [21] have pointed out that one of the most promising spatial discretization methods is probably a HR scheme in which the interpolation stencil is aligned with the ordinate directions. Such bounded skew high-order resolution (SHR) schemes have recently been developed for CFD [22]. The objective of this work is to demonstrate the application of these SHR schemes to the discrete ordinates method and to investigate their performance. We consider only transparent or gray media, but the extension to nongray media is straightforward.

The discrete ordinates method is briefly described in the next section, and the discretization schemes employed in this work are presented. Several test problems are then solved for two- and three-dimensional enclosures with transparent, emitting–absorbing or emitting–absorbing–scattering media. The main conclusions are drawn in the last section.

2. THE DISCRETE ORDINATES METHOD

2.1. *The Radiative Transfer Equation*

The radiative transfer equation may be written as follows for an emitting–absorbing–scattering gray medium [23]:

$$\frac{dI(\mathbf{s})}{ds} = -\beta I(\mathbf{s}) + \kappa I_b + \frac{\sigma_s}{4\pi}\int_{4\pi} I(\mathbf{s}')\phi(\mathbf{s}', \mathbf{s})\, d\Omega'. \tag{1}$$

In this equation, $I(\mathbf{s})$ is the radiation intensity in direction $\mathbf{s}$; I_b is the blackbody radiation intensity, κ, β, and σ_s are the absorption, extinction, and scattering coefficients of the medium, respectively; and $\phi(\mathbf{s}', \mathbf{s})$ is the scattering-phase function. The ratio $\phi(\mathbf{s}', \mathbf{s})/4\pi$ represents the probability that radiation propagating in direction $\mathbf{s}'$ and confined within solid angle $d\Omega'$ is scattered through the angle $\mathbf{s}' \cdot \mathbf{s}$ into the direction $\mathbf{s}$ confined within solid angle $d\Omega$.

The boundary condition for a gray surface that emits and reflects diffusely, given in Ref. [23], is

$$I_w(\mathbf{s}) = \varepsilon I_{bw} + \frac{\rho}{\pi} \int_{\mathbf{n}\cdot\mathbf{s}'<0} I(\mathbf{s}')|\mathbf{n} \cdot \mathbf{s}'| \, d\Omega', \tag{2}$$

where $I_w(\mathbf{s})$ is the radiation intensity leaving the boundary surface, $I(\mathbf{s}')$ is the radiation intensity in the $\mathbf{s}'$ direction arriving at that surface, I_{bw} is the blackbody radiation intensity at the temperature of the boundary surface, ε is the surface emissivity, ρ is the surface reflectivity, and $\mathbf{n}$ is the outward unit vector normal to the surface.

2.2. *The Discrete Ordinate Equations*

In the discrete ordinates method, the radiative transfer equation is replaced by a discrete set of M coupled differential equations that describe the radiation intensity field along M directions. Integrals over solid angles are replaced by a quadrature of order M, yielding

$$\frac{dI^m}{ds} = -\beta I^m + \kappa I_b + \frac{\sigma_s}{4\pi} \sum_{j=1}^{M} I^j \phi(\mathbf{s}_j, \mathbf{s}_m) w_j, \tag{3}$$

where the superscript m denotes the mth direction and w_j is the quadrature weight of the jth direction. In the present work, level symmetric S_N quadratures were used ($M = N(N+2)$). The S_4, S_6, and S_8 quadratures satisfy sequential odd moments, and the S_{10} and S_{12} quadratures satisfy sequential even moments [24].

The boundary condition expressed by Eq. (2) is discretized as

$$I_w^m = \varepsilon I_{bw} + \frac{\rho}{\pi} \sum_{\substack{j \\ (\mathbf{n}\cdot\mathbf{s}_j<0)}} I^j |\mathbf{n} \cdot \mathbf{s}_j| w_j, \quad \mathbf{n} \cdot \mathbf{s}_m > 0. \tag{4}$$

Spatial discretization of the discrete ordinate equations is carried out using the finite-volume approach. Equation (3) is integrated over a typical control volume, and the Gauss divergence theorem is applied. The terms on the right-hand side of Eq. (3) are assumed to be constant over the control volume. The in-scattering term (last one of Eq. (3)) is split into two parts, one that accounts for the contribution of the mth direction, which is treated implicitly, and the other accounting for all the other directions, which is treated explicitly [10]. For a Cartesian coordinate system and for a direction m with direction cosines ξ^m, η^m, and μ^m, this yields the discretized equations

$$\begin{aligned} &|\xi^m| A_x \left(I^m_{x,out} - I^m_{x,in}\right) + |\eta^m| A_y \left(I^m_{y,out} - I^m_{y,in}\right) + |\mu^m| A_z \left(I^m_{z,out} - I^m_{z,in}\right) \\ &\quad = \left(-\beta I_P^m + \frac{\sigma_s}{4\pi} I_P^m \phi(\mathbf{s}_m, \mathbf{s}_m) w_m + S_P^m\right) V, \end{aligned} \tag{5}$$

where

$$S_P^m = \kappa I_{bP} + \frac{\sigma_s}{4\pi} \sum_{\substack{j=1 \\ (j\neq m)}}^{M} I_P^j \phi(\mathbf{s}_j, \mathbf{s}_m) w_j. \tag{6}$$

In these equations, A_x, A_y, and A_z are the areas of the control-volume faces normal to the x, y, and z directions, respectively; V is the volume; and S_P^m is the modified source term of the radiative transfer equation at grid node P and for direction m. The subscripts of the cell face intensities represent the direction (x, y, or z) and the upstream (*in*) or downstream (*out*) face. If $\xi^m > 0$, then $I_{x,in}^m$ and $I_{x,out}^m$ are the intensities at the west and east cell faces, respectively. Conversely, if $\xi^m < 0$, then $I_{x,in}^m$ and $I_{x,out}^m$ are the intensities at the east and west cell faces, respectively. The radiation intensities at the cell faces are unknowns and must be related to radiation intensities at neighboring grid nodes. This may be accomplished by using any of the schemes referred to in the introduction. Here, the family of SHR schemes [22] is considered. To our knowledge, such schemes had never been applied before to the radiative transfer equation. However, it is useful to first address the HR schemes, which have also been used for comparison purposes.

2.3. *Bounded High-Order Resolution Schemes*

High-order resolution schemes express the dependent variable (the radiation intensity in the present case) at a cell face f as a function of its values at three neighboring grid nodes, two upstream and one downstream from the cell face. These are denoted by the subscripts U, C, and D, as shown in Fig. 1, and are referred to as upstream, central, and downstream grid nodes, respectively. Figure 1 represents two-dimensional control volumes for the sake of clarity. The normalized variable formulation introduced by Leonard [25] has provided a good framework for the development of HR schemes. This has been extended to nonuniform grids in Ref. [26], where it is referred to as normalized variable and space formulation. According to this formulation, a normalized radiation intensity $\tilde{I}$ and a normalized coordinate $\tilde{x}$ are defined as

$$\tilde{I} = \frac{I - I_U}{I_D - I_U}, \tag{7a}$$

$$\tilde{x} = \frac{x - x_U}{x_D - x_U}. \tag{7b}$$

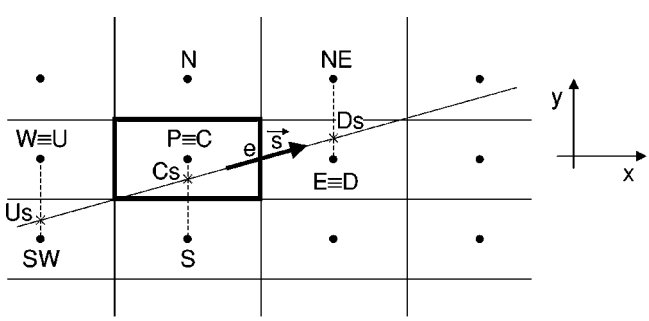

FIG. 1. Typical control volume. The radiation intensity at the east cell face is computed from its values at upstream (U), central (C), and downstream (D) grid nodes in HR schemes, and upstream (Us), central (Cs), and downstream (Ds) points along **s** direction in SHR schemes.

Bounded schemes must satisfy a boundedness criterion originally described in [16]. This criterion is directly applicable to the radiative transfer equation, as reported in Ref. [21], and may be summarized as follows.

(i) The function $\tilde{I}_f = f(\tilde{I}_C)$ is continuous.
(ii) $\tilde{I}_C \le \tilde{I}_f \le 1$ for $0 \le \tilde{I}_C \le 1$.
(iii) $\tilde{I}_f = \tilde{I}_C$ for $\tilde{I}_C < 0$ or $\tilde{I}_C > 1$.

The step scheme in the normalized variable and space formulation is written as $\tilde{I}_f = \tilde{I}_C$. Therefore, it is a bounded scheme but only first-order accurate. In fact, it has been shown that a necessary and sufficient condition for a scheme to be second-order accurate is to be defined by a functional relationship passing through the point $(\tilde{x}_C, \tilde{x}_f)$, or (0.5, 0.75) for uniform grids [16, 26]. If, in addition, the slope of the functional relationship at that point is equal to $\tilde{x}_f(\tilde{x}_f - 1)/[\tilde{x}_C(\tilde{x}_C - 1)]$, or 0.75 for uniform grids, then the scheme is third-order accurate [16, 26]. Many schemes satisfying the boundedness criterion have been developed since this criterion was formulated (see, e.g., Ref. [27]). Among them, the CLAM [20], MUSCL [19], and SMART schemes were used in the present work. These schemes are given by the following functional relationships [26].

CLAM:

$$\tilde{I}_f = \frac{\left(\tilde{x}_C^2 - \tilde{x}_f\right)}{\tilde{x}_C(\tilde{x}_C - 1)}\tilde{I}_C + \frac{(\tilde{x}_f - \tilde{x}_C)}{\tilde{x}_C(\tilde{x}_C - 1)}\tilde{I}_C^2 \quad \text{for } 0 < \tilde{I}_C < 1, \tag{8a}$$

$$\tilde{I}_f = \tilde{I}_C \quad \text{elsewhere.} \tag{8b}$$

MUSCL:

$$\tilde{I}_f = \frac{2\tilde{x}_f - \tilde{x}_C}{\tilde{x}_C}\tilde{I}_C \quad \text{for } 0 < \tilde{I}_C < \tilde{x}_C/2, \tag{9a}$$

$$\tilde{I}_f = \tilde{I}_C + (\tilde{x}_f - \tilde{x}_C) \quad \text{for } \tilde{x}_C/2 \le \tilde{I}_C < 1 + \tilde{x}_C - \tilde{x}_f, \tag{9b}$$

$$\tilde{I}_f = 1 \quad \text{for } 1 + \tilde{x}_C - \tilde{x}_f \le \tilde{I}_C < 1, \tag{9c}$$

$$\tilde{I}_f = \tilde{I}_C \quad \text{elsewhere.} \tag{9d}$$

SMART:

$$\tilde{I}_f = \frac{\tilde{x}_f(1 - 3\tilde{x}_C + 2\tilde{x}_f)}{\tilde{x}_C(1 - \tilde{x}_C)}\tilde{I}_C \quad \text{for } 0 < \tilde{I}_C < \tilde{x}_C/3, \tag{10a}$$

$$\tilde{I}_f = \frac{\tilde{x}_f(1 - \tilde{x}_f)}{\tilde{x}_C(1 - \tilde{x}_C)}\tilde{I}_C + \frac{\tilde{x}_f(\tilde{x}_f - \tilde{x}_C)}{(1 - \tilde{x}_C)} \quad \text{for } \frac{\tilde{x}_C}{3} \le \tilde{I}_C < \frac{\tilde{x}_C}{\tilde{x}_f}(1 + \tilde{x}_f - \tilde{x}_C), \tag{10b}$$

$$\tilde{I}_f = 1 \quad \text{for } \frac{\tilde{x}_C}{\tilde{x}_f}(1 + \tilde{x}_f - \tilde{x}_C) \le \tilde{I}_C < 1, \tag{10c}$$

$$\tilde{I}_f = \tilde{I}_C \quad \text{elsewhere.} \tag{10d}$$

It is worth pointing out that the results of the CLAM scheme are not necessarily bounded for nonuniform grids. Although uniform grids were used in this work, the upstream grid node (U) lies on the boundary surface for control volumes whose upstream cell face is on the boundary surface. Therefore, the normalized coordinates at the downstream cell face are $\tilde{x}_f = 2/3$ and $\tilde{x}_C = 1/3$, which differ from the values at interior control volumes: $\tilde{x}_f = 3/4$

and $\tilde{x}_C = 1/2$. The functional relationship of the CLAM scheme in normalized coordinates is a second-degree polynomial in the range $0 < \tilde{I}_C < 1$, given by Eq. (8a). Therefore, since $\tilde{I}_f(0) = 0$ and $\tilde{I}_f(1) = 1$, the boundedness criterion will be violated if $d\tilde{I}_f/d\tilde{I}_C = 0$ in that range (i.e., there will be points where $\tilde{I}_f > 1$). It is easy to verify that the derivative will vanish at a point in the range $0 < \tilde{I}_C < 1$ if the condition $\tilde{x}_f > \tilde{x}_C(2 - \tilde{x}_C)$ holds. If the grid is uniform, this condition is never verified for interior control volumes, and the scheme is bounded. However, in a nonuniform grid, that condition may be verified and the boundedness criterion violated. The condition is also verified if $\tilde{x}_f = 2/3$ and $\tilde{x}_C = 1/3$. However, it is easy to enforce boundedness by setting $\tilde{I}_f = 1$ if the second-degree polynomial in the range $0 < \tilde{I}_C < 1$ yields a value greater than 1. This simple strategy was employed in all CLAM and skew CLAM results reported here.

2.4. *Bounded Skew High-Order Resolution Schemes*

In SHR schemes, the dependent variable at a cell face f is also determined from its values at three neighboring points, two upstream and one downstream from the cell face. However, these are not grid nodes but points located at the intersection of the direction of propagation of radiation, **s**, with the grid lines, as shown in Fig. 1. The radiation intensity at these points, denoted by Us, Cs, and Ds, is calculated from linear interpolation of the radiation intensity at the neighboring grid nodes. For example, the radiation intensity at point Us in Fig. 1 is computed from linear interpolation of the radiation intensity at grid nodes $W \equiv U$ and SW. In three-dimensional problems, a bilinear interpolation is used. A more accurate interpolation scheme is likely to be needed to preserve the accuracy of schemes of order greater than second. Among the schemes employed here, only the SMART scheme may present such a high order of accuracy. However, this has not been observed in the calculations reported in [21], and therefore a linear interpolation was always used in the present work.

The normalization of the radiation intensity and coordinate are based on the radiation intensities and coordinates along the **s** direction:

$$\tilde{I}_s = \frac{I - I_{Us}}{I_{Ds} - I_{Us}}, \tag{11a}$$

$$\tilde{s} = \frac{s - s_{Us}}{s_{Ds} - s_{Us}}. \tag{11b}$$

The normalized coordinate $\tilde{s}$ is calculated from distances measured along direction **s**, rather than along the coordinate axes. The radiation intensity at cell face f is computed using Eqs. (8), (9), or (10), with $\tilde{I}_s$ and $\tilde{s}$ substituted for $\tilde{I}$ and $\tilde{x}$, respectively.

The boundedness criterion mentioned above ensures that the radiation intensity at the cell face is bounded with respect to the interpolated radiation intensities at Us, Cs, and Ds. However, it is not necessarily bounded with respect to the neighboring grid nodes of cell face f (U, C, and D). Therefore, wiggles in the computed radiation field may still occur. To avoid an unbounded solution it is necessary to proceed as follows [22]. First, the radiation intensity at a cell face is calculated as described (i.e., from the SHR scheme applied to the points lying along the direction of propagation of the radiation intensity). Then, it is checked if the computed cell face radiation intensity satisfies the boundedness criterion with respect to the neighboring grid nodes (U, C, and D). If it does, then no additional corrections are needed; otherwise, the boundedness criterion is enforced using the HR scheme instead of

the SHR one. At cell faces coincident with downstream boundaries, there is no downstream grid node. Therefore, the step scheme was used in that case.

2.5. *Solution Method*

The SHR schemes were implemented using the deferred correction procedure [28]. According to this method, the downstream cell face radiation intensities are expressed as the radiation intensities computed from the step scheme plus a correction equal to the difference between the radiation intensities computed from the SHR scheme and the step scheme:

$$I^m_{f,out} = I^m_{f,out,step} + \left(I^m_{f,out,SHR} - I^m_{f,out,step}\right). \tag{12}$$

The contribution from the step scheme is treated implicitly while the correction term in parenthesis is treated explicitly. Inserting Eq. (12) into Eq. (5), noting that $I^m_{f,out,step} = I^m_P$, and solving for I^m_P yields

$$I^m_P = \frac{|\xi^m|A_x\, I^m_{x,in} + |\eta^m|A_y\, I^m_{y,in} + |\mu^m|A_z\, I^m_{z,in} + S^m_P V + S^m_{dc}}{|\xi^m|A_x + |\eta^m|A_y + |\mu^m|A_z + \left(\beta - \dfrac{\sigma_s}{4\pi}\phi(\mathbf{s}_m, \mathbf{s}_m)w_m\right)V}, \tag{13}$$

where the deferred correction term, S^m_{dc}, is defined as

$$S^m_{dc} = |\xi^m|A_x\left(I^m_P - I^m_{x,out}\right) + |\eta^m|A_y\left(I^m_P - I^m_{y,out}\right) + |\mu^m|A_z\left(I^m_P - I^m_{z,out}\right). \tag{14}$$

All the cell face radiation intensities in Eqs. (13) and (14) are obtained from the SHR scheme, and so no explicit reference to the scheme is included in the subscript. The values of $I^m_{x,out}$, $I^m_{y,out}$, and $I^m_{z,out}$ are computed from Eq. (11) and Eqs. (8), (9), or (10), depending on the specific SHR scheme employed, using the radiation intensities computed at the previous iteration for downstream grid nodes, and at the current iteration for upstream grid nodes. The values of $I^m_{x,in}$, $I^m_{y,in}$, and $I^m_{z,in}$ are available either from the boundary conditions, if an upstream cell face coincides with a boundary, or from the calculations performed for the upstream control volumes.

In each iteration, and for each direction, the surface radiosities and the blackbody radiation intensities are either known or guessed based on the values computed in the previous iteration. The surface irradiation is neglected in the first iteration. The radiation intensities at every control volume and direction are determined by a point-by-point method applied to Eq. (13). For each direction, calculations start from a control volume at one of the corners of the enclosure. That corner is selected from the sign of the direction cosines, in such a way that the cell faces that merge at that corner are upstream cell faces coincident with the boundaries of the enclosure. The radiation intensity at those faces is available from the boundary conditions, enabling the calculation of the radiation intensity at the first control volume using Eq. (13). The solution proceeds in the direction of orientation of the direction cosines, visiting all the control volumes. Then, similar calculations are performed for all the other directions. After all the directions have been treated, the radiation intensities leaving the boundary surfaces are updated using the boundary conditions, Eq. (4). The iteration process continues until the convergence criterion has been satisfied.

If the temperature field is not known, it must be determined from the simultaneous solution of the energy conservation equation and the radiative transfer equation. In the

problems addressed here it is assumed that radiation is the dominant mode of heat transfer; the others are neglected. Therefore, conservation of energy may be expressed as [23]

$$\nabla \cdot \mathbf{q} = \kappa(4\sigma T^4 - G), \tag{15}$$

where $\mathbf{q}$ is the radiative heat flux vector, T is the temperature of the medium, and σ is the Stefan–Boltzmann constant. The incident radiation, G, is given by

$$G = \int_{4\pi} I \, d\Omega \approx \sum_{j=1}^{M} w_j \, I^j. \tag{16}$$

In the case of radiative equilibrium (i.e., $\nabla \cdot \mathbf{q} = 0$), the temperature field is updated at every iteration from Eqs. (15) and (16).

2.6. *Computational Details*

In the case of a transparent medium, the convergence criterion employed in this work was

$$\frac{\sum_i \sum_j \sum_k \sum_{m=1}^{M} \left| \left(I_{i,j,k}^m\right)^n - \left(I_{i,j,k}^m\right)^{n-1} \right|}{\sum_i \sum_j \sum_k \sum_{m=1}^{M} \left(I_{i,j,k}^m\right)^n} < \delta, \tag{17}$$

where n and $n-1$ denote the present and the previous iterations, respectively, and the summations extend over all the control volumes and directions. The prescribed tolerance, δ, was set to 10^{-8} in the two-dimensional problems and to 2×10^{-5} in the three-dimensional problem.

In the case of a participating medium, the convergence criterion was

$$\max \left\{ \frac{|G^n - G^{n-1}|}{G^n} \right\} < \delta. \tag{18}$$

The maximum over all the control volumes of the quantity within the braces must decrease below a tolerance taken as 10^{-4}.

It was found that during the iterative solution procedure, switching between the SHR and the HR scheme often occurs, causing convergence difficulties. To prevent this, if at a given cell face the SHR scheme does not satisfy the boundedness criterion with respect to the neighboring grid nodes more than n_{BC} times during the iterative process, then the HR scheme is used at that cell face in all the following iterations. However, the SHR scheme is still used at other cell faces where the n_{BC} limit is not attained. Several tests were performed to find the optimum value of n_{BC}, and it was found that $n_{\mathrm{BC}} = 2$ or $n_{\mathrm{BC}} = 3$ is usually the best choice.

The use of the SHR scheme instead of the HR one generally degrades the convergence rate. Therefore, it was found useful to employ the HR scheme until the error measure considered in the convergence criterion decreases to a prescribed level, typically 10^{-3}, and then to switch to the SHR scheme.

It was also verified, as reported in the next section, that the gain in accuracy is limited if the SHR scheme is used instead of the HR one for directions that make a small angle with a coordinate axis. This has a well-known counterpart in CFD, where the upwind scheme may only originate significant false diffusion if the direction of the velocity is oblique to the grid lines. Therefore, the SHR scheme was used in two-dimensional problems if $\pi/6 \le tg^{-1}(|\eta^m|/|\xi^m|) \le \pi/3$, while the HR scheme was employed otherwise. In three-dimensions, the SHR scheme was used only if one or more of the angles $tg^{-1}(|\eta^m|/|\xi^m|)$, $tg^{-1}(|\mu^m|/|\xi^m|)$, and $tg^{-1}(|\mu^m|/|\eta^m|)$ lie in the range $[\pi/6, \pi/3]$.

Finally, to achieve a converged solution, it was often necessary to underrelax the deferred correction term given by Eq. (14). This is required for both the HR and the SHR schemes, although the SHR schemes generally require stronger underrelaxation. Although a converged solution has been obtained in the problems tested, there is no guarantee that convergence will be obtained for all problems.

3. RESULTS AND DISCUSSION

The results presented and discussed in this section are organized into three subsections, according to the radiative properties of the medium. First, two- and three-dimensional enclosures with a transparent medium are studied. Second, the medium is assumed to emit and absorb, but no scattering is considered. The temperature of the medium is prescribed or, alternatively, radiative equilibrium is assumed. Finally, an emitting–absorbing and scattering medium is studied, including isotropic and anisotropic scattering. In all problems, the enclosure has one hot wall, while the others walls are cold. This causes a discontinuity of the boundary radiation intensity at the edges of the hot wall, which propagates to the radiation intensity field within the enclosure. In such cases, skewed discretization schemes are expected to be more accurate. However, if the radiation intensity along the boundary is either constant or varies smoothly, then no major advantage of skewed schemes is expected.

3.1. *Transparent Medium*

The first problem consists of a two-dimensional square enclosure (dimensions $L_x = L_y = 1$) with a transparent medium, black walls, $I_{bw} = 1$ at the bottom wall, and $I_{bw} = 0$ elsewhere. A single direction of propagation of radiation intensity with $\xi^m = 0.5$ and $\eta^m = \sqrt{3}/2$ and a 6×6 uniform grid are considered. The grid and the direction were chosen to enable a comparison between our results and those reported in [13]. The exact solution is given by $I^m = 1$ below the dashed lines in Fig. 2, and $I^m = 0$ above those lines. The radiation intensity is discontinuous along the dashed lines, as a result of the discontinuity between the bottom and left boundary wall intensities.

Figure 2 shows the radiation intensity field computed using the step, diamond, SMART, and skew SMART schemes, as well as the exponential high-order schemes used in Refs. [12, 13]. The solutions obtained with the diamond and the exponential high-order schemes have been taken from [13]. The step scheme solution is bounded but exhibits strong numerical smearing, as expected, while the diamond scheme solution presents unphysical oscillations and overshoots, but substantially reduces the numerical smearing. The other four solutions given in Fig. 2 completely remove oscillations, undershoots, and overshoots and present only moderate numerical smearing.

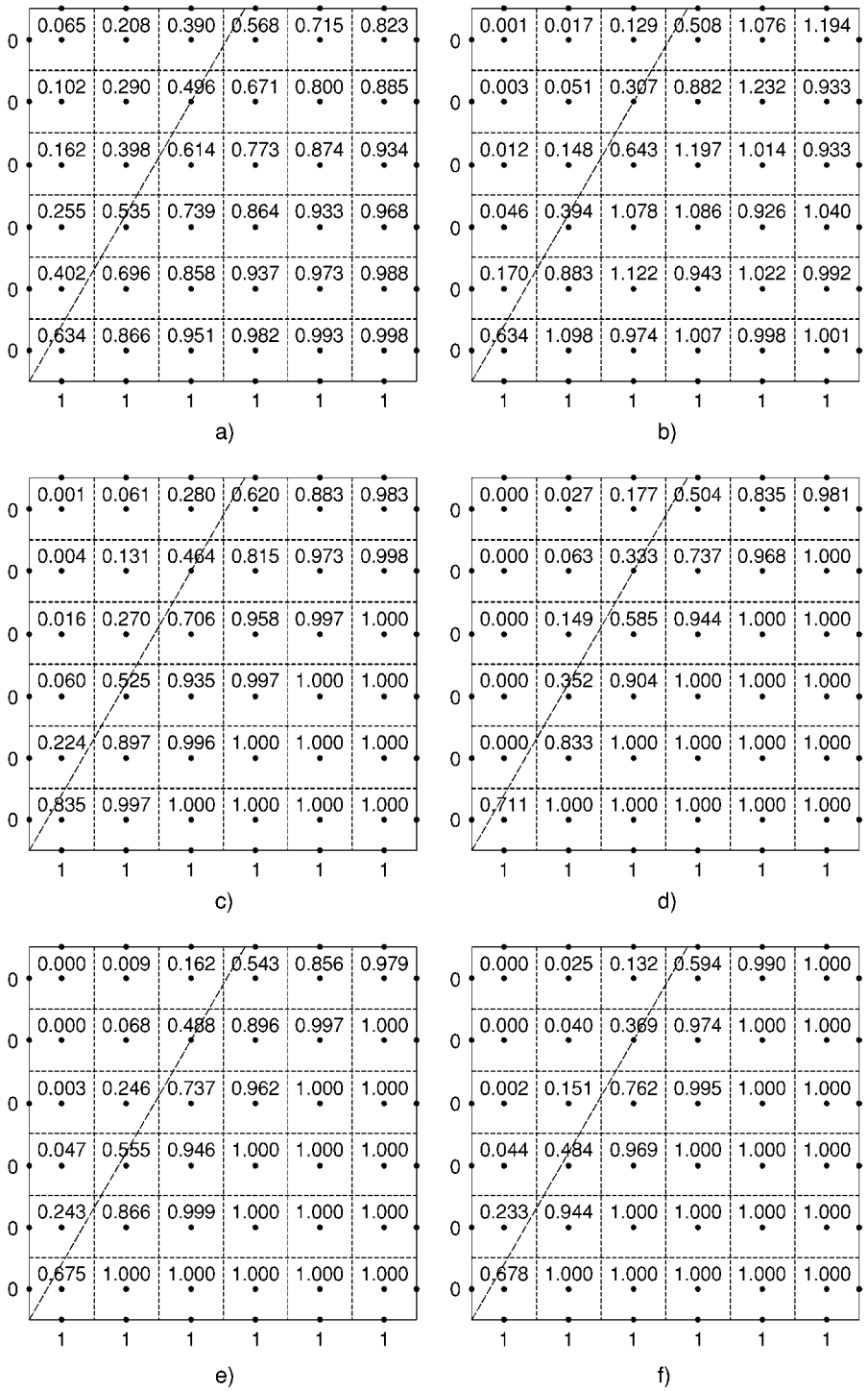

FIG. 2. Computed radiation intensity fields in a two-dimensional square enclosure with a transparent medium ($\xi^m = 0.5$, $\eta^m = \sqrt{3}/2$, 6×6 uniform grid). The exact radiation intensity is 1 below the dashed lines and 0 above them. (a) Step scheme; (b) diamond scheme (results taken from Ref. [13]); (c) exponential high-order scheme (results taken from Ref. [13]); (d) exponential high-order scheme (results taken from Ref. [13]); (e) SMART; and (f) skew SMART.

TABLE I

Average Absolute Error of Radiation Intensity in Direction $\xi^m = 0.5$, $\eta^m = \sqrt{3}/2$ in a Two-Dimensional Square Enclosure with a Transparent Medium (6×6 Uniform Grid)

Scheme	E_{I1}^m	E_{I2}^m
Step	0.1998	0.1540
Diamond[a]	0.1224	0.0837
Exponential high-order scheme [12][a]	0.0943	0.0553
Exponential high-order scheme with linear interpolation [13][a]	0.0943	0.0608
Exponential high-order scheme with cubic interpolation [13][a]	0.0843	0.0564
CLAM	0.1019	0.0559
MUSCL	0.0958	0.0499
SMART	0.0904	0.0445
Skew CLAM	0.0797	0.0351
Skew MUSCL	0.0741	0.0302
Skew SMART	0.0724	0.0283

[a] Radiation intensity field taken from Ref. [13].

The average absolute error of the radiation intensity in direction m may be used to quantify the solution accuracy. It is given by

$$E_I^m = \frac{\sum_{i=1}^{I} \sum_{j=1}^{J} \left| I_{i,j}^m - I_{i,j,exact}^m \right|}{I \times J}, \tag{19}$$

where I and J are the number of grid nodes along x and y directions, respectively. A relative error could not be used here, since the radiation intensity may be zero. Although the radiation intensity is always greater than zero in practical problems, in the fictitious case of a cold wall ($I_{bw} = 0$) and a transparent medium, the radiation intensity at an arbitrary point of the enclosure is zero for directions leaving from the cold wall. The exact value of the radiation intensity at a control volume may be taken either as the grid node value or as the mean value over that control volume, yielding two different average absolute errors, denoted by E_{I1}^m and E_{I2}^m, respectively. These are shown in Table I for several spatial discretization schemes. In addition to the schemes that produce the solutions displayed in Fig. 2, Table I includes results for the exponential high-order scheme with cubic interpolation of the upstream radiation intensity [13], the CLAM, MUSCL, skew CLAM, and skew MUSCL schemes. The average errors of the exponential schemes are comparable to those of the HR schemes and significantly lower than that of the diamond scheme. The step scheme is by far the least accurate scheme, while the SHR schemes are the most accurate ones. The SMART scheme is slightly more accurate than the MUSCL, and this is slightly more accurate than the CLAM. This is also true for the SHR version of these schemes. These conclusions do not depend on the way I_{exact} was obtained (i.e., on whether E_{I1}^m or E_{I2}^m is considered). Therefore, only E_{I1}^m is used from now on, and the subscript 1 is removed for conciseness.

The predicted radiation intensity along the vertical symmetry plane, $x = 0.5$, for direction $\xi^m = \eta^m = 0.5774$ and a 11×11 uniform grid is shown in Fig. 3. The numerical smearing is very significant for the step scheme, as expected, since this direction makes an angle of

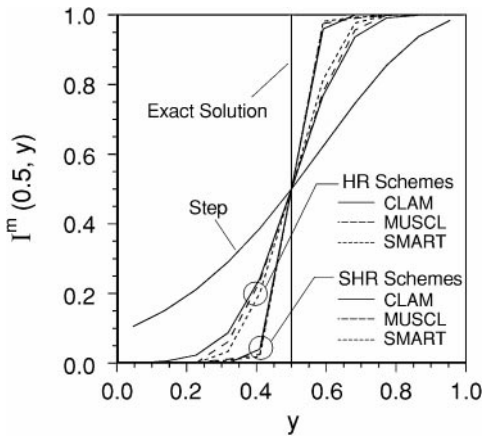

FIG. 3. Radiation intensity profile along the vertical symmetry plane of a two-dimensional square enclosure with a transparent medium ($\xi^m = \eta^m = 0.5774$, 11×11 uniform grid).

45° with the grid lines. The HR schemes perform much better, while the SHR schemes further approach the sharp discontinuity of the exact solution at $y = 0.5$. All the HR and SHR schemes are bounded and oscillation free. This is best seen in Fig. 4, where three-dimensional perspectives of the radiation intensity field are displayed. The results of the CLAM and MUSCL schemes (HR and SHR versions) are not shown, since they are very close to the results of the SMART scheme. These results are identical to those obtained in the classical CFD problem of convection of a step profile in a prescribed oblique velocity field.

The influence of the grid size on the average absolute error of the radiation intensity field in direction $\xi^m = \eta^m = 0.5774$ is shown in Fig. 5. The error decreases with grid refinement, as expected, but the rate of convergence is low. Although the HR schemes are second- (CLAM, MUSCL) or third-order (SMART) accurate, the observed rate of convergence only marginally exceeds that of the first-order accurate step scheme. This is related to the discontinuity in the radiation intensity field, which prevents the schemes from behaving according to their formal rate of convergence. Other reasons may be responsible for the degradation of the rate of convergence, as discussed in [21]. These include the limiting required to prevent oscillations, the propagation to all downstream locations of local errors that may arise when a lower order approximation is required to enforce boundedness, and the unalignment of the stencils with respect to the ordinate directions. The last reason is eliminated in the SHR schemes, which show a faster rate of convergence than the HR schemes.

Up to now attention has been focused on the radiation intensity for a single direction. If all the directions are taken into account, an average absolute error of the radiation intensity field may be defined as

$$E_I = \frac{\sum_{m=1}^{M} E_I^m}{M}. \tag{20}$$

The influence of the grid size and order of quadrature on the average absolute error E_I are shown in Fig. 6. In the first case, the S_8 quadrature was used (Fig. 6a), while in the last one a 40×40 uniform grid was employed (Fig. 6b). Although the emphasis of this work is on the

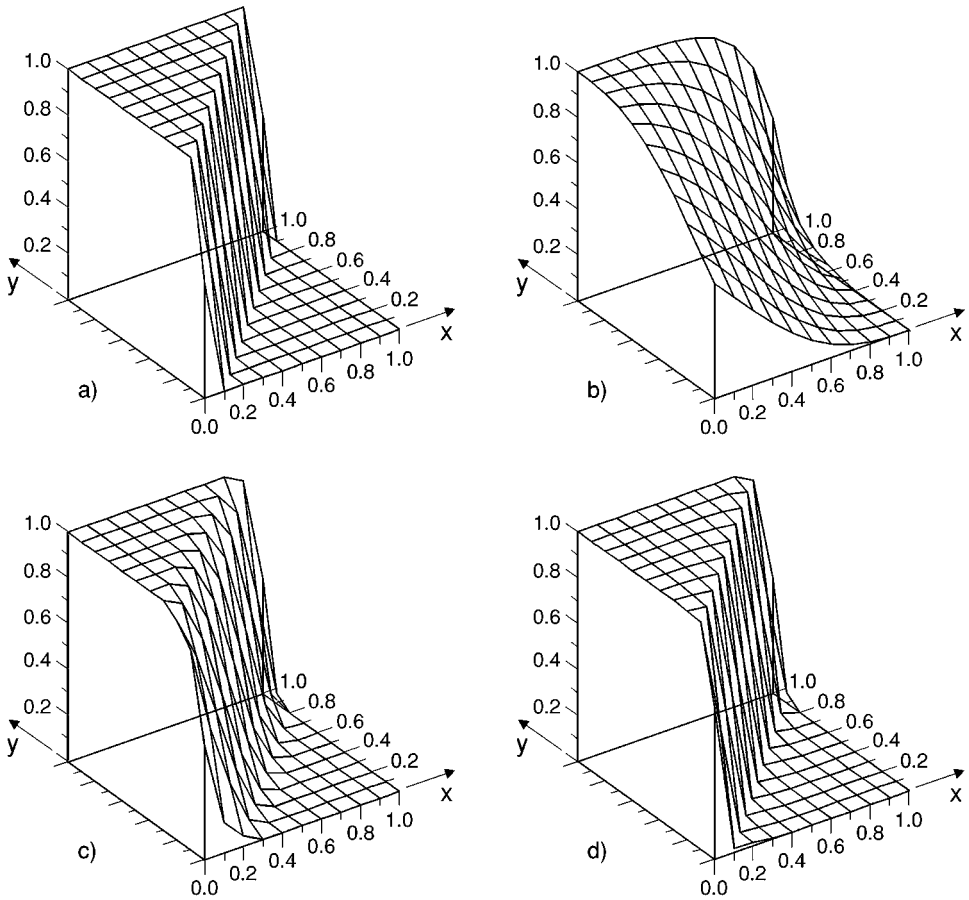

FIG. 4. Radiation intensity field in a two-dimensional square enclosure with a transparent medium ($\xi^m = \eta^m = 0.5774$, 11×11 uniform grid). (a) Exact solution; (b) step scheme; (c) SMART; and (d) skew SMART.

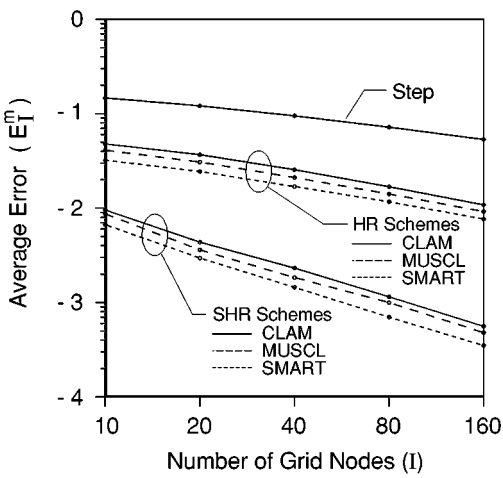

FIG. 5. Average absolute error of the radiation intensity in direction $\xi^m = \eta^m = 0.5774$ as a function of grid size.

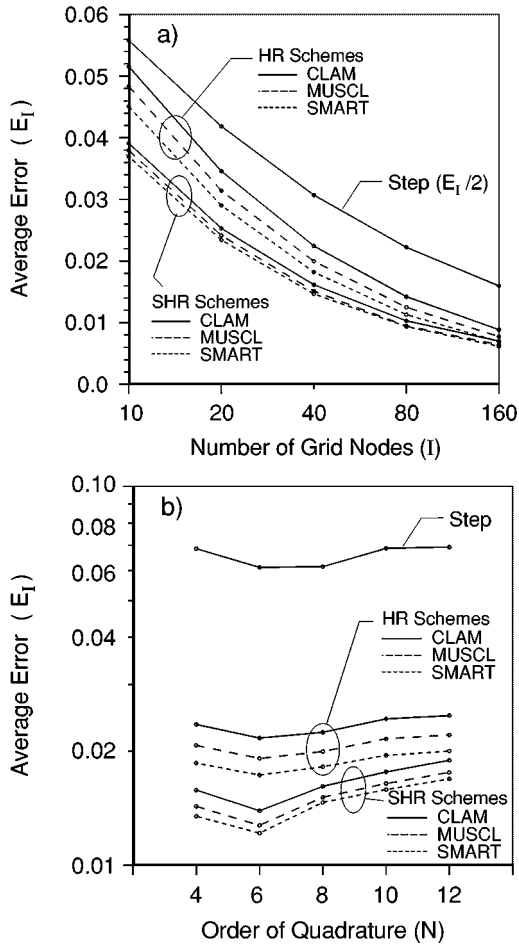

FIG. 6. Average absolute error of the radiation intensity field in a two-dimensional square enclosure with a transparent medium as a function of grid size (a) and order of quadrature (b).

spatial discretization rather than on the angular discretization, it is interesting to investigate whether or not the SHR schemes behave like the HR schemes when the angular discretization is refined. In fact, the superior accuracy of the SHR over the HR schemes is enhanced when the angle between the direction of propagation of radiation and the coordinate lines, which depends on the order of quadrature, approaches a maximum. The results show that the relative behavior of the different spatial discretization schemes is independent of the grid size and order of quadrature. The error of the step scheme exceeds that of the other schemes by a factor larger than 2, while the SHR schemes are the most accurate ones. The ratio of the error of the step scheme to the error of the other schemes increases with the grid refinement. This shows that the step scheme has the lowest rate of convergence, as expected. However, all the other schemes exhibit similar rates of convergence, contrary to what was observed for direction $\xi^m = \eta^m = 0.5774$.

To clarify these trends, the average absolute errors for every direction are summarized in Table II for a 10×10 uniform grid and a S_8 quadrature. Similar conclusions would be obtained from other grids or quadratures. The results of the MUSCL and SMART scheme are not shown, since they perform similarly to the CLAM scheme. Although there are

TABLE II
Average Absolute Error of Radiation Intensity in a Two-Dimensional Square Enclosure with a Transparent Medium (10 × 10 grid, S_8 Quadrature)

			E_I^m			
m	ξ^m	η^m	Step	CLAM	Skew CLAM	Skew CLAM all directions
1	0.9796	0.1423	0.06607	0.03795	0.03795	0.03743
2	0.8040	0.1423	0.07516	0.04184	0.04184	0.04162
3	0.8040	0.5774	0.17820	0.08197	0.05914	0.05914
4	0.5774	0.1423	0.09209	0.04809	0.04809	0.04508
5	0.5774	0.5774	0.14668	0.04790	0.00955	0.00955

10 directions per octant, it is sufficient to look at the results of the directions listed in Table II, because in this problem the errors for directions (ξ, η) and (η, ξ) are equal. The error for $m = 5$, the direction that makes an angle of 45° with the coordinate lines, decreases by a factor of 5 when the SHR scheme is used instead of the HR scheme. The correspondent error for $m = 3$ decreases only by a factor of 1.4, while the errors for the remaining directions do not change, since the angles they make with the grid lines do not lie in the range $[\pi/6, \pi/3]$; i.e., the HR scheme is active. The errors that would be obtained if the SHR scheme were always used (i.e., if the range $[\pi/6, \pi/3]$ were extended to $[0, \pi/2]$), are listed in the last column of Table II. The marginal decrease in error observed for directions 1, 2, and 4 demonstrates that it is only worth using the skewed scheme if $tg^{-1}(|\eta^m|/|\xi^m|)$ is relatively close to $\pi/4$, as it was here. The error of the SHR scheme in direction $m = 5(\xi^m = \eta^m)$ is much smaller than that in the other directions. Therefore, the average absolute error of the SHR schemes is dominated by the errors in the other directions, and so the rate of convergence is similar to that of the HR schemes.

The next test problem is similar to the first one, but the geometry is a three-dimensional cubic enclosure ($L_x = L_y = L_z = 1$). The walls are black with $I_{bw} = 1$ at the bottom wall and $I_{bw} = 0$ elsewhere, and the medium is transparent. The average absolute error of the radiation intensity field, given by Eq. (20), as a function of grid size is shown in Fig. 7. The S_8 quadrature was used. The results are qualitatively identical to those presented in Fig. 6a for the two-dimensional enclosure.

3.2. *Emitting–Absorbing, Nonscattering Medium*

The two-dimensional enclosure studied in the previous section is considered again, with the same boundary conditions, but containing an emitting–absorbing, nonscattering medium with an emissive power of unity ($I_{bw} = 1/\pi$) and an absorption coefficient of 1.0. In the case of participating media it is more useful to evaluate the solution accuracy using the incident radiation rather than the radiation intensity. Moreover, since the incident radiation is always greater than zero, relative errors may be used. Therefore, an average relative error of the incident radiation was taken to quantify the solution accuracy [21]:

$$E_G = \frac{\sum_{i=1}^{I} \sum_{j=1}^{J} \frac{|G - G_{exact}|}{G_{exact}}}{I \times J}. \tag{21}$$

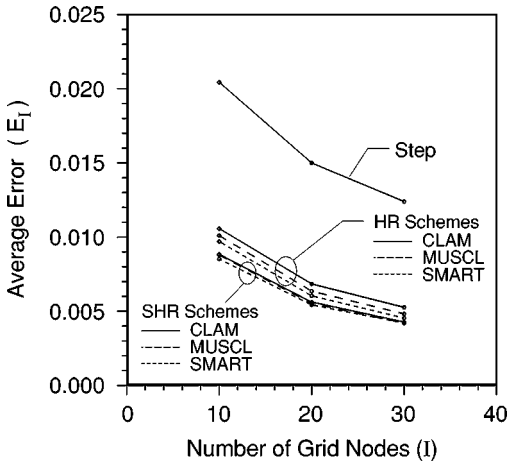

FIG. 7. Average absolute error of the radiation intensity field in a three-dimensional cubic enclosure with a transparent medium as a function of grid size.

Here, G_{exact} is taken from the exact solution of the discrete ordinate equations (Eq. (3)), reported in [29], rather than from the exact solution of the radiative transfer equation (Eq. (1)). This ensures that the computed error is a consequence of the spatial discretization error, and is not influenced by ray effects. The results presented below were obtained using a 40×40 uniform grid and the S_8 quadrature, except in the cases where the influence of grid size or quadrature are investigated. The influence of the spatial discretization scheme and grid size on the solution error E_G is shown in Fig. 8. The results are consistent with those reported for the transparent medium. All the SHR schemes perform similarly, and are more accurate than the correspondent HR schemes. The accuracy of the SHR schemes in a 10×10 grid is comparable to that of the step scheme in a 80×80 grid (notice that the errors of the step scheme marked in Fig. 8 have been divided by a factor of 2).

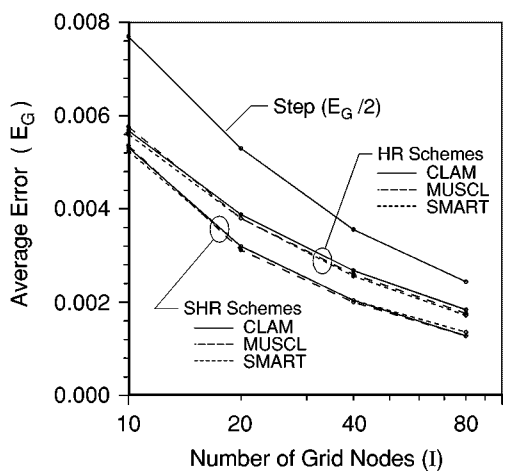

FIG. 8. Average relative error of the incident radiation in a two-dimensional square enclosure with an emitting–absorbing medium as a function of grid size.

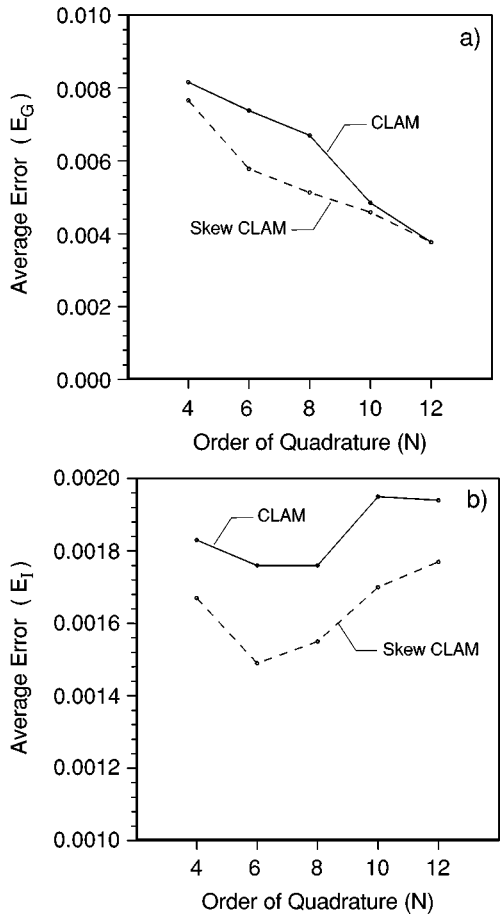

FIG. 9. Average errors in a two-dimensional square enclosure with an emitting–absorbing medium as a function of the order of quadrature. (a) Average relative error of the incident radiation, E_G. (b) Average absolute error of the radiation intensity field, E_I.

The influence of the order of quadrature on the incident radiation error E_G is shown in Fig. 9a. Only the results of the CLAM and skew CLAM schemes are shown, but they are very close to the results of the other HR and SHR schemes. The skew CLAM is more accurate than the CLAM for S_6 and S_8 quadratures, as expected. However, the results of the two schemes are similar if S_4, S_{10}, or S_{12} quadratures are used. This may be explained by a compensation of errors in the calculation of the radiation intensity. In fact, all the ordinate directions contribute to the incident radiation, according to Eq. (16). If the radiation intensity for some directions is overestimated while for others it is underestimated, the two opposite contributions may cancel each other out, yielding an accurate value of the incident radiation. This explanation is supported by the average absolute error of the radiation intensity, E_I, shown in Fig. 9b, which is always lower for the SHR scheme, despite the order of quadrature.

The influence of the absorption coefficient of the medium is shown in Fig. 10. In the case of an optically thick medium, the terms $S_P^m\ V$ and $\beta\ V$ are the dominant ones on the numerator and denominator of Eq. (13), respectively. The ratio of these two terms is equal to I_b because the medium does not scatter. This explains why the average incident radiation

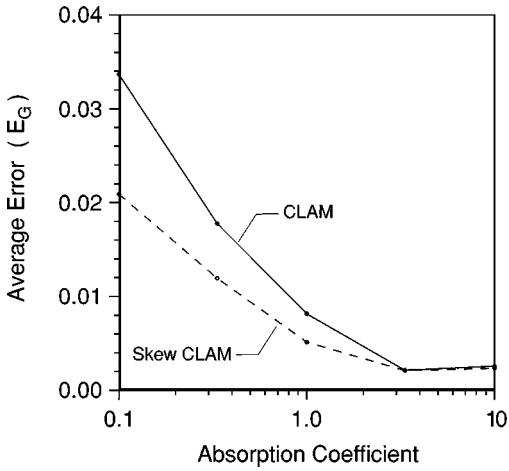

FIG. 10. Average relative error of the incident radiation in a two-dimensional square enclosure with an emitting–absorbing medium as a function of the absorption coefficient of the medium.

error for optically thick media is small, approximately constant, and weakly dependent on the spatial discretization scheme. Conversely, if the medium is optically thin, those two terms are small, and the spatial discretization scheme employed in the calculation of the cell face intensities becomes important. Therefore, the average error of the incident radiation is larger than in the case of an optically thin medium, and the higher accuracy of the SHR scheme compared to the HR scheme becomes evident.

Figure 11 shows the average error of the radiation intensity field as a function of the emissivity of the boundary surface. In this case there is no analytical solution available if $\varepsilon < 1$. Therefore, G_{exact} was approximated by the numerical solution obtained from a very fine grid (320×320 grid nodes) and the CLAM scheme. The results show that E_G increases with the increase in the boundary emissivity. In fact, if ε increases, so does the radiation

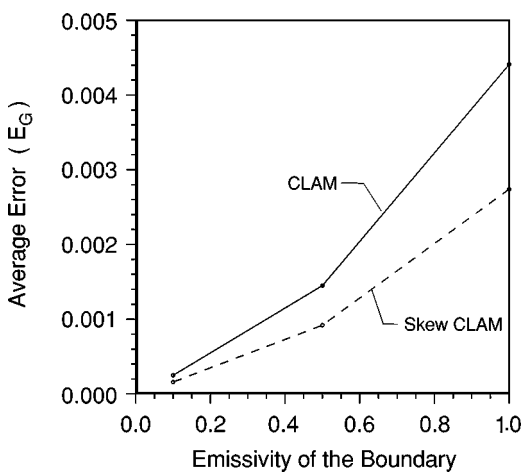

FIG. 11. Average relative error of the incident radiation in a two-dimensional square enclosure with an emitting–absorbing medium as a function of the emissivity of the boundary surface.

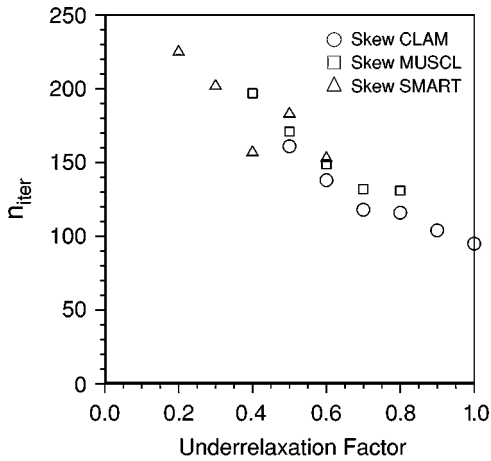

FIG. 12. Number of iterations required for convergence as a function of the underrelaxation factor.

intensity at the bottom surface. Therefore, the discontinuity of the radiation intensity at the bottom left and right corners, which is the main cause of the spatial discretization errors, becomes sharper. The skew CLAM results are more accurate than the CLAM ones, particularly for high boundary surface emissivities, since the ratio $E_G(\text{CLAM})/E_G(\text{skew CLAM})$ slightly increases with the increase in ε.

Although the SHR schemes have consistently proved to be more accurate than the HR ones, they also have some drawbacks. Their implementation is more tedious, they are more sensitive to the underrelaxation factor, and they are more computationally demanding, particularly for fine grids. The sensitivity to the underrelaxation factor is illustrated in Fig. 12. Convergence is faster with a high underrelaxation factor, but it is possible that convergence is not achieved if that factor is too high. In this test case, the highest underrelaxation factors that enable convergence were 1, 0.8, and 0.6 for the skew CLAM, skew MUSCL, and skew SMART schemes, respectively. This behavior is the expected one, and similar to that of the HR schemes. The number of iterations, n_{iter}, and the central processing unit (CPU) time, t, required for convergence are shown in Fig. 13. The number of iterations increases moderately with grid size for the HR schemes, but that increase is much more significant for the SHR schemes. Therefore, if the grid is refined, the computational requirements of the SHR schemes increase due to both the number of grid nodes and the number of iterations. Fortunately, since the SHR schemes are quite accurate, there is no need to use very fine grids. Whether or not the higher accuracy of the SHR schemes over the HR schemes compensates for their higher computational requirements is likely to be problem dependent. This is also true for the different HR and SHR schemes; i.e., the SMART scheme is generally more accurate than the MUSCL scheme, and this is generally more accurate than the CLAM scheme, but the higher accuracy is associated with more CPU time required for convergence.

The computational cost, or economy, of the different schemes may be evaluated for a given problem by considering equal accuracy as a basis for determining economy [16]. The average relative error of the incident radiation, taken as a measure of accuracy, is plotted in Fig. 14 as a function of CPU time for the different discretization schemes and meshes. This allows the comparison of the accuracy of the different schemes for a given amount of CPU time, as well as the estimation of the CPU time required to attain a given level of accuracy. Figure 14 shows

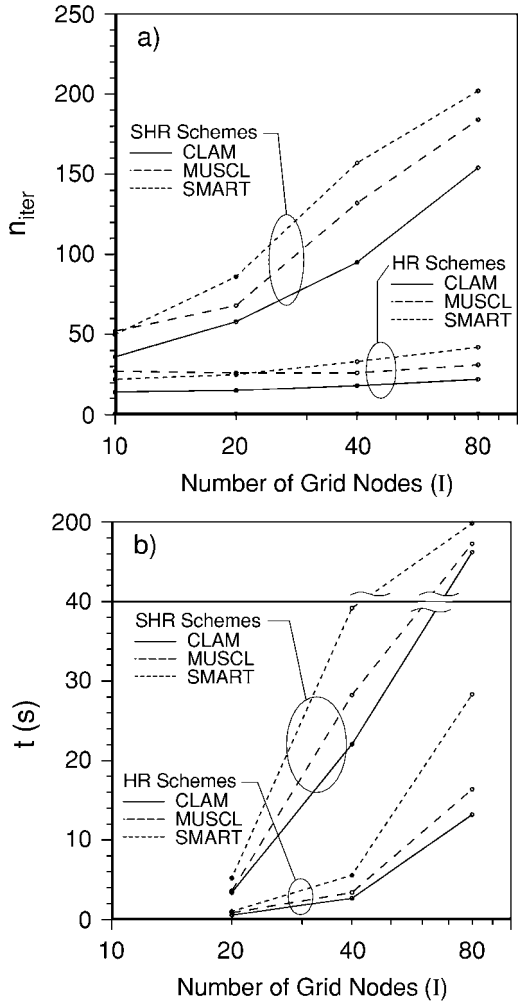

FIG. 13. (a) Number of iterations and (b) CPU time(s) required for convergence.

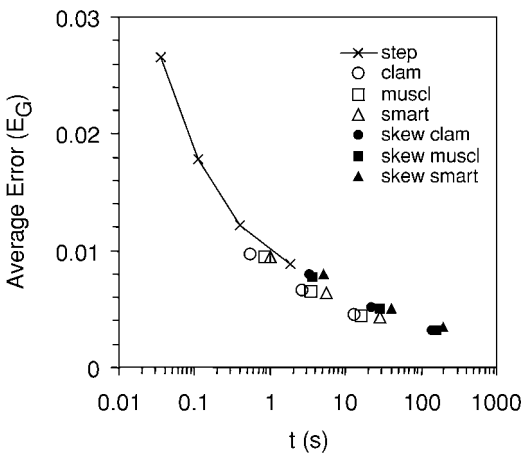

FIG. 14. Average relative error of the incident radiation as a function of the CPU time for a two-dimensional square enclosure with an emitting–absorbing medium.

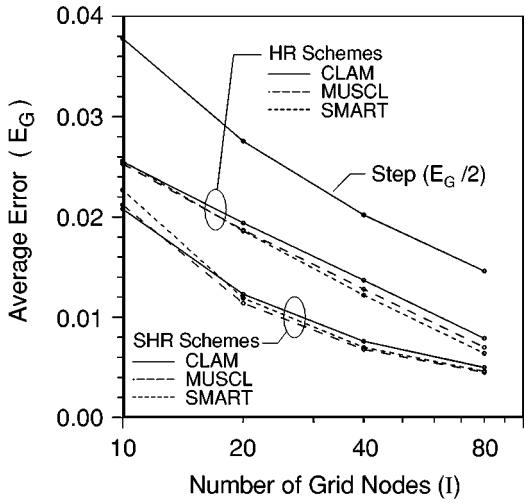

FIG. 15. Average relative error of the incident radiation in a two-dimensional square enclosure with an emitting–absorbing medium in radiative equilibrium.

that the HR schemes are slightly more economical than the SHR schemes for this problem. The STEP scheme is also relatively economical in this problem, because all the walls of the enclosure are black, the temperature of the medium is prescribed, and there is no scattering. Therefore, it does not require an iterative procedure, unlike the HR and SHR schemes.

The same geometrical configuration and boundary conditions are considered in the next problem, but radiative equilibrium is assumed. Hence, the energy equation (Eq. (15)) is solved together with the radiative transfer equation. Since no exact solution is available, G_{exact} is approximated as above. The S_8 quadrature is used again in this problem. The average relative error of the incident radiation as a function of the grid size is shown in Fig. 15. The results are qualitatively similar to those shown in Fig. 8, concerning a medium with prescribed emissive power. The errors are larger in the present case because the temperature of the medium is obtained from the solution of the energy equation, and so errors in the temperature field influence the incident radiation. The gain in accuracy obtained by using the SHR schemes instead of the HR ones is also larger in this problem. The rate of convergence of the SHR schemes seems slower than that of the HR schemes, contrary to what would be expected. However, this may be due to the approximation used to estimate G_{exact}. Figure 16 shows the number of iterations and the CPU time required for convergence as a function of the grid size. It does not reveal significant differences between the cases of radiative equilibrium and prescribed emissive power. Figure 17 shows that in this test case, the computational cost to achieve a given level of accuracy is similar for the HR and SHR schemes, while the STEP scheme is much less economical, as expected.

3.3. *Emitting–Absorbing–Scattering Medium*

The problem studied in Section 3.2 with prescribed emissive power of the medium is considered again. But now the medium scatters isotropically. As in the previous section, the present calculations were carried out using a 40×40 uniform grid and the S_8 quadrature, and G_{exact} was approximated by the CLAM solution in a 320×320 uniform grid. The average relative error of the incident radiation as a function of the scattering albedo is

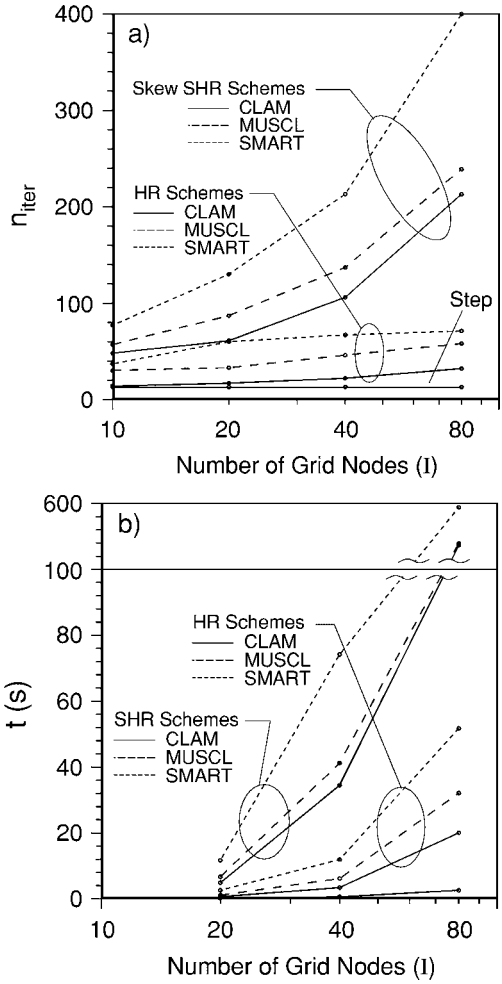

FIG. 16. (a) Number of iterations and (b) CPU time(s) required for convergence in the case of a two-dimensional square enclosure with an emitting–absorbing medium in radiative equilibrium.

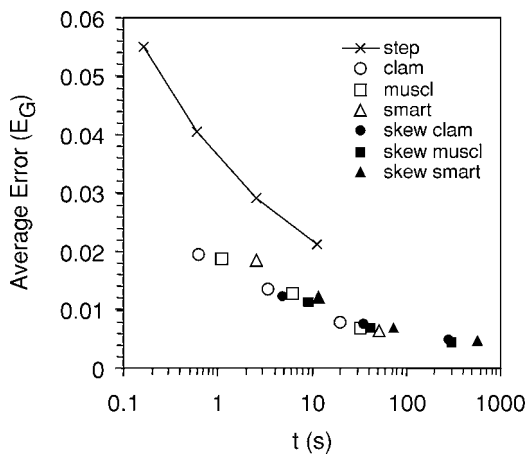

FIG. 17. Average relative error of the incident radiation as a function of the CPU time for a two-dimensional square enclosure with an emitting–absorbing medium in radiative equilibrium.

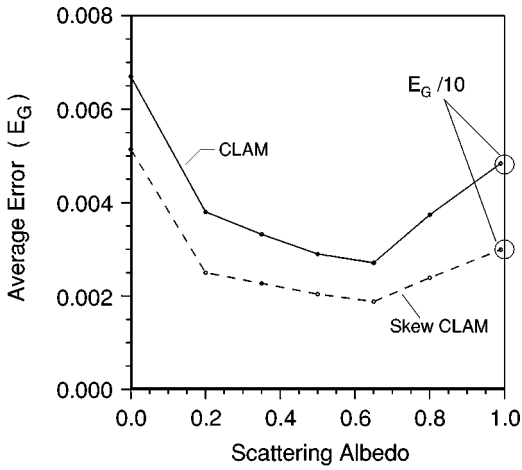

FIG. 18. Average relative error of the incident radiation in a two-dimensional square enclosure with an emitting–absorbing, isotropically scattering medium.

shown in Fig. 18. The scattering albedo, ω, is the ratio of the scattering to the extinction coefficients ($\omega = \sigma_s/\beta$). The absorption coefficient was maintained constant and equal to 1.0, while the scattering coefficient was allowed to change. The results show that the errors are largest for low or high values of ω. The skew CLAM scheme is more accurate than the CLAM scheme, as in the case of nonscattering and transparent media. The gain in accuracy (40–60%) is marginally influenced by the scattering albedo. Other SHR and HR schemes perform similarly.

Finally, the medium was assumed to scatter anisotropically. The phase functions F1, F2, B1, and B2 described in [30] were considered. The results summarized in Table III reveal that the gain in accuracy by using the skew CLAM scheme is substantial (more than 40%) for all the phase functions.

Nowadays, the simulation of reactive flows in geometries of relevance in industry is often carried out using unstructured meshes. Although the application of SHR schemes to unstructured meshes is not addressed in this work, no difficulties are foreseen in that application. If Cartesian coordinates are used, the upstream, central, and downstream grid nodes required in HR schemes are readily available, while SHR schemes require an

TABLE III

Average Relative Error of the Incident Radiation in a Two-Dimensional Square Enclosure with an Emitting–Absorbing, Anisotropically Scattering Medium

	E_G	
Phase function[a]	CLAM	Skew CLAM
F1	0.00382	0.00218
F2	0.00291	0.00208
B1	0.00296	0.00207
B2	0.00302	0.00208

[a] See Ref. [30].

interpolation, as illustrated in Fig. 1. However, in the case of unstructured grids, an interpolation is required for both HR and SHR schemes. Therefore, it is tempting to speculate that the advantage of SHR over HR schemes might be more obvious in unstructured grids, but the present lack of evidence recommends simply stating that this issue should be investigated in future work.

4. CONCLUSION

Numerical smearing is one of the main sources of error in the discrete ordinates method for the solution of the radiative transfer equation. This error is particularly relevant if the step scheme is employed. Bounded high-order resolution schemes substantially decrease the numerical smearing. However, the stencil used in the spatial discretization is aligned with the coordinate axes. In this work, bounded skew high-order resolution schemes have been employed which use a stencil aligned with the direction of the propagation of radiation. Several radiative transfer problems in enclosures were solved. Both transparent and participating media were considered, including nonscattering, isotropically scattering, and anisotropically scattering media. In all cases, one of the walls of the enclosure was hot and the others were cold. It was found that skewed schemes yield more accurate results, especially for the radiation intensity along directions oblique to the grid lines, and for optically thin media. The skewed schemes are more computationally demanding, particularly for fine grids. However, these are not generally required due to the accuracy of the schemes. Whether the superior accuracy of skewed schemes compensates for their higher computational requirements is likely to be problem dependent.

ACKNOWLEDGMENT

The PRAXIS XXI Program of the Portuguese Ministry of Science and Technology supported this work under contract PRAXIS/P/EME/12034/1998.

REFERENCES

1. R. Viskanta and M. P. Mengüç, Radiation heat transfer in combustion systems, *Prog. Energy Combust. Sci.* **13**, 97 (1987).
2. B. G. Carlson and K. D. Lathrop, Transport theory—The method of discrete-ordinates, in *Computing Methods in Reactor Physics*, edited by H. Greenspan, C. N. Kelber, and D. Okrent (Gordon & Breach, New York, 1968), 171.
3. W. A. Fiveland, Discrete-ordinates solution of the radiative transport equation for rectangular enclosures, *J. Heat Transfer* **106**, 699 (1984).
4. K. D. Lathrop, Ray effects in discrete ordinates equations, *Nucl. Sci. Eng.* **32**, 357 (1968).
5. J. C. Chai, H. S. Lee, and S. V. Patankar, Ray effect and false scattering in the discrete ordinates method, *Numer. Heat Transfer B* **24**, 373 (1993).
6. M. A. Ramankutty and A. L. Crosbie, Modified discrete ordinates solution of radiative transfer in two-dimensional rectangular enclosures, *J. Quant. Spectrosc. Radiat. Transfer* **57**, 107 (1997).
7. J. C. Chai, S. V. Patankar, and H. S. Lee, Evaluation of spatial differencing practices for the discrete-ordinates method, *J. Thermophys. Heat Transfer* **8**, 140 (1994).
8. K. D. Lathrop, Spatial differencing of the transport equation: Positivity vs. accuracy, *J. Comput. Phys.* **4**, 475 (1969).
9. A. S. Jamaluddin and P. J. Smith, Predicting radiative transfer in rectangular enclosures using the discrete ordinates method, *Combust. Sci. Technol.* **59**, 321 (1988).

10. J. C. Chai, H. S. Lee, and S. V. Patankar, Improved treatment of scattering using the discrete ordinates method, *J. Heat Transfer* **116**, 260 (1994).
11. N. El Wakil and J. F. Sacadura, Some improvements of the discrete ordinates method for the solution of the radiative transport equation in multidimensional anisotropically scattering media, *ASME HTD* **103**, 119 (1992).
12. G. D. Raithby and E. H. Chui, A finite-volume method for predicting a radiant heat transfer in enclosures with participating media, *J. Heat Transfer* **112**, 415 (1990).
13. K.-B. Cheong and T.-H. Song, An alternative discrete ordinates method with interpolation and source differencing for two-dimensional radiative transfer problems, *Numer. Heat Transfer B* **32**, 107 (1997).
14. S.-H. Seo and T.-K. Kim, Study on interpolation schemes of the discrete ordinates interpolation method for three-dimensional radiative transfer with nonortoghonal grids, *J. Heat Transfer* **120**, 1091 (1998).
15. D. R. Rousse, G. Gautier, and J. F. Sacadura, An upwinding procedure for numerical radiation heat transfer, in *Proceedings of the 3rd European Thermal Sciences Conference, Heidelberg, Germany, September 2000*, edited by E. W. P. Hahne, W. Heidemann, and K. Spindler (Edizioni ETS, Pisa, 2000), p. 587.
16. P. H. Gaskell and A. K. C. Lau, Curvature compensated convective transport: SMART, a new boundedness preserving transport algorithm, *Int. J. Numer. Methods. Fluids* **8**, 617 (1988).
17. F. Liu, H. A. Becker, and A. Pollard, Spatial differencing schemes of the discrete-ordinates method, *Numer. Heat Transfer B* **30**, 23 (1996).
18. A. Harten, High resolution schemes for hyperbolic conservation laws, *J. Comput. Phys*. **49**, 357 (1983).
19. B. Van Leer, Towards the ultimate conservation difference scheme. V. A second-order sequel to Godunov's method, *J. Comput. Phys*. **32**, 101 (1979).
20. B. Van Leer, Towards the ultimate conservation difference scheme. II. Monoticity and conservation combined in a second-order scheme, *J. Comput. Phys*. **14**, 361 (1974).
21. J. P. Jessee and W. A. Fiveland, Bounded, high-resolution differencing schemes applied to the discrete ordinates method, *J. Thermophy. Heat Transfer* **11**, 540 (1997).
22. F. Moukalled and M. Darwish, A new family of streamline-based very-high-resolution schemes, *Numer. Heat Transfer B* **32**, 299 (1997).
23. M. F. Modest, *Radiative Heat Transfer* (McGraw-Hill, New York, 1993).
24. W. A. Fiveland, The selection of discrete ordinate quadrature sets for anisotropic scattering, *ASME HTD* **160**, 89, 1991.
25. B. P. Leonard, A survey of finite differences with upwinding for numerical modelling of the incompressible convection diffusion equation, in *Computational Techniques in Transient and Turbulent Flow*, edited by C. Taylor and K. Morgan (Pineridge, Swansea, Wales, 1981), Vol. 2, p. 1.
26. M. S. Darwish and F. H. Moukalled, Normalized variable and space formulation for high-resolution schemes, *Numer. Heat Transfer B* **26**, 79 (1994).
27. B. P. Leonard, Bounded higher-order upwind multidimensional finite-volume convection-diffusion algorithms, in *Advances in Numerical Heat Transfer*, edited by W. J. Minkowycz and E. M. Sparrow (Taylor & Francis, London, 1997), Vol. 1, p. 1.
28. P. K. Khosla and S. G. Rubin, A diagonally dominant second order accurate implicit scheme, *Comput. Fluids* **2**, 207 (1974).
29. J. P. Jessee, W. A. Fiveland, L. H. Howell, P. Colella, and R. B. Pember, An adaptive mesh refinement algorithm for the radiative transport equation, *J. Comput. Phys*. **139**, 380 (1998).
30. T.-K. Kim and H. Lee, Effect of anisotropic scattering on radiative heat transfer in two-dimensional rectangular enclosures, *Int. J. Heat Mass Transfer* **31**, 1711 (1988).